

# Estimate of the Black-Hole Mass and Orbital Inclination from the Radial-Velocity Curve of the X-Ray Binary Cyg X-1

M. K. Abubekerov<sup>1</sup>, E. A. Antokhina<sup>2</sup>, and A. M. Cherepashchuk<sup>1,2</sup>

<sup>1</sup>*Moscow State University, Vorob'evy gory, Moscow, 119899 Russia*

<sup>2</sup>*Sternberg Astronomical Institute, Moscow State University, Universitetskii pr. 13, Moscow, 119899 Russia*

Received January 5, 2004; in final form, January 9, 2004

**Abstract**—The results of a statistical approach to interpreting a master radial-velocity curve for the X-ray binary Cyg X-1 are presented. The dependence of the mass of the X-ray component  $m_x$  on the mass of the optical component  $m_v$  is obtained in a Roche model. A method for estimating the orbital inclination from the radial-velocity curve is described. In contrast to the situation for a pointlike optical star, both the amplitude and shape of the radial-velocity curve changes as a function of the orbital inclination  $i$  in the case of a tidally deformed star with a complex temperature distribution over its surface. Thus, high-accuracy radial-velocity curves can be used to impose constraints on the mass and orbital inclination of the black hole:  $i < 45^\circ$ . Using the information on the optical light curve, radius, and luminosity of the optical star, we estimate  $31^\circ < i < 44^\circ$  and  $8.5M_\odot < m_x < 13.6M_\odot$ . © 2004 MAIK “Nauka/Interperiodica”.

## 1. INTRODUCTION

A new method for determining the component-mass ratio and orbital inclination of an X-ray binary from the orbital variability of the absorption-line profiles in the spectrum of the optical star was proposed by Antokhina and Cherepashchuk [1] and Shahbaz [2]. The dependence of the absorption-line profile on the phase of the orbital period is due to the tidal deformation of the star's shape and the complex temperature distribution over its surface due to gravitational darkening and the effect of X-ray heating. High-resolution spectra ( $R = \lambda/\Delta\lambda = 50\,000$ ) are necessary to apply this method to X-ray novae in their quiescent state. In principle, such spectra can be obtained using modern 8–10 m telescopes, but with considerable difficulties.

The Cyg X-1 system, which is composed of a O9.7Iab supergiant and a black hole, is sufficiently bright ( $V = 9.5^m$ ) to obtain high-resolution spectra suitable for investigations of fine effects in the optical star's rotation [3] and obtaining spectroscopic estimates of the parameters of the optical using model atmospheres [4].

A large number of measurements of the radial velocity of the optical star in the Cyg X-1 system with moderate spectral resolution have been accumulated up to the present. These can be used to construct a high-accuracy radial-velocity curve, which should contain the averaged effects of the orbital variability in the absorption line profiles, as is described in [1, 2]. Therefore, it is of interest to try to estimate simultaneously the black-hole mass and orbital inclination of

Cyg X-1 using a high-accuracy mean radial-velocity curve.

In contrast to the model with two point masses, both the amplitude and shape of the radial-velocity curve change with variations in the orbital inclination of an X-ray binary containing a tidally deformed optical star. Wilson and Sofia [5] were the first to draw attention to this dependence. This effect makes it possible to estimate both the mass and the orbital inclination of the system based on a high-accuracy radial-velocity curve of Cyg X-1.

## 2. OBSERVATIONAL MATERIAL

A master radial-velocity curve was compiled from the spectral data of [6–12], which were obtained in 1973–1997. Since the test undertaken in [13] demonstrated that the theoretical radial velocities for the He I 4713 Å and H $\gamma$  absorption lines are very similar, the velocities determined from both hydrogen and He I lines were included in the master radial-velocity curve. Although the spectral data were separated by considerable time intervals, they agree with each other very well (Fig. 1). We took the orbital period of the X-ray binary Cyg X-1 to be 5<sup>d</sup>599829, as follows from the analysis of a long series of observations [12].

The observed velocities were corrected for the systemic velocity before their inclusion in the radial-velocity curve. The systemic velocity of the close binary derived from the spectral data of [6–12] is

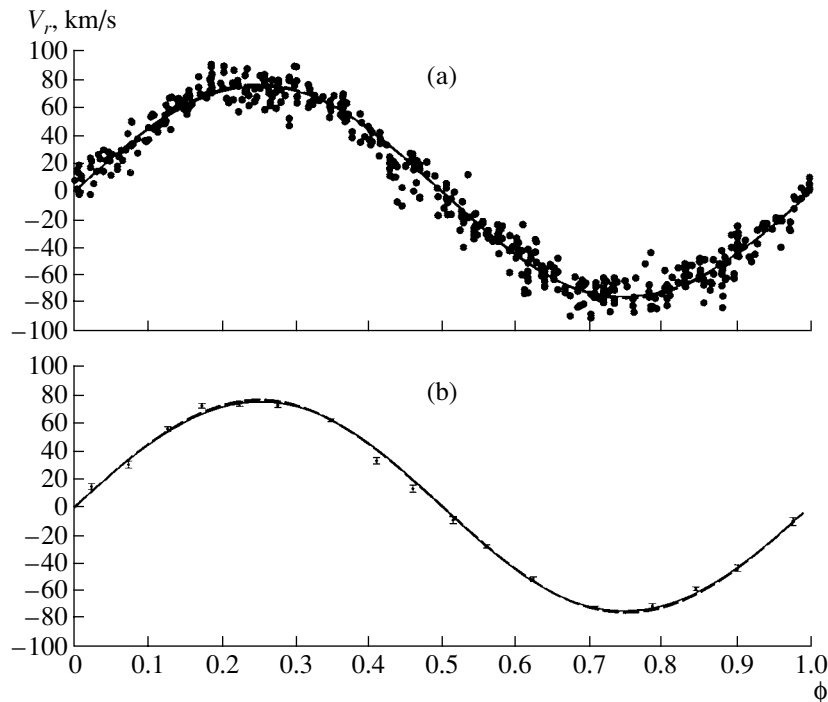


**Fig. 1.** (a) Master observed radial-velocity curve for the optical star in the X-ray binary Cyg X-1. Filled circles represent radial velocities derived from absorption lines of hydrogen and HeI. For comparison, theoretical radial-velocity curves for the Roche model (solid) and point-mass model (dashed) are also presented. These curves were obtained for  $m_x = 10.86M_\odot$ , which corresponds to the minimum residual in the Roche model with  $m_v = 20M_\odot$  calculated using method 2 (i.e., excluding the mean observed radial velocities at phases 0.4–0.6) and with an orbital inclination of  $35^\circ$ . The parameters of the Roche model are summarized in Table 2. (b) Radial velocities averaged over phase intervals (the average radial velocities within phase intervals are presented by the filled circles). For comparison, theoretical radial-velocity curves for the Roche model (solid) and point-mass model (dashed) with  $m_v = 20M_\odot$ ,  $m_x = 10.86M_\odot$ , and  $i = 35^\circ$  are also presented.

presented in Table 1. Let us discuss in more detail each of these cited works.

A set of summer observations of HDE 226868 carried out in 1973 using a 2.54-m telescope are presented in [6]. A total of 17 spectra at 6100–6800 Å with a dispersion of 20 Å/mm were obtained. The radial velocities were determined from the HeI 6678 Å absorption line.

The spectral data presented in [7] were collected from 1972 to 1975. The exposure time for these spectra was 20–65 min. A total of 85 spectra were obtained: 23 with a dispersion of 39 Å/mm obtained using a 2.1-m Cassegrain telescope and 62 with a dispersion of 63 Å/mm obtained using a 0.9-m Cassegrain telescope. The radial velocity was derived from absorption lines of hydrogen H9, H8, Hδ, Hγ, helium HeI 4026 Å, and HeI 4471 Å.

Spectra obtained from 1971 to 1981 using a 1.88-m telescope are presented in [8]. A total of 78 spectra at 3700–4920 Å with dispersions of 12 and 16 Å/mm were recorded. The radial velocity

was measured using both absorption lines of hydrogen (Hβ, Hγ, Hδ, Hε, and H8–H16) and helium (HeI 3819.606, 4009.270, 4026.189, 4120.812, 4143.759, 4168.971, 4387.928, 4387.928, 4471.507, and 4713.143 Å).

Spectral observations obtained from 1980 to 1984 are presented in [9]. A total of 84 spectra were obtained on a 1.22-m telescope with a dispersion of 40 Å/mm (or 0.6 Å per diode), a 1.83-m telescope with a dispersion of 15 Å/mm (or 0.231 Å per diode), and a 3.6-m telescope with a dispersion of 2.4 Å/mm (or 0.036 Å per diode). The radial velocities were measured separately using absorption lines of hydrogen and helium. The radial velocity for the hydrogen absorption lines was determined as the weighted mean of the velocities for the Hβ, Hγ, and Hδ lines. The radial velocity for the helium lines was determined as the weighted mean of the velocities for the HeI 4009.270, 4026.189, 4120.812, 4143.759, 4387.928, 4471.477, 4713.143, 4921.929, 5015.675, and 5047.736 Å absorption lines.

Observations of HDE 226868 carried out in 1985–1986 are described in [10]. A total of 14 spectra

**Table 1.** Observation epoch, element whose line was used to measure the radial velocity, number of spectra, and systemic radial velocity of the optical component of Cyg X-1

JD 24400000+	Element	Number of spectra	$\gamma$ velocity, km/s	Reference
41844–41290	HeI	17	−3.6	[6]
42205–42910	H, HeI	85	−5.3	[7]
41213–44795	H	78	−2.5	[8]
	HeI	78	−4.2	[8]
44513–45895	H	56	−10.4	[9]
	HeI	84	−5.6	[9]
46332–46635	HeI	14	−10.5	[10]
50228–50255	H	35	−7.5	[11]
	HeI	35	−2.9	[11]
50615–50677	HeI	20	−2.1	[12]

were obtained on a 2.1-m telescope at 6500–6710 Å with a dispersion of 0.14 Å per pixel. The exposure time for each spectrum varied from 1–3 h. The signal-to-noise ratio per pixel was  $S/N = 100–300$ . The radial velocity was measured using the HeI 6678 Å absorption line.

Observations of the optical component of Cyg X-1 carried out in 1996 using the Isaac Newton Telescope are presented in [11]. A total of 37 spectra were obtained at 4100–4900 Å with a dispersion of 0.8 Å/mm, exposure times of 100–200 s, and  $S/N > 100$ . The radial velocity was determined relative to a standard spectrum of Cep 19 using a cross-correlation method. The velocity was measured separately for the absorption lines of hydrogen and HeI. The HeI 4387.928, 4471.477, 4713.143, and 4921.929 Å absorption lines were used.

Spectra obtained using a Coudé spectrograph of the 2.6-m telescope of the Crimean Astrophysical Observatory are presented in [12]. A total of 20 spectra with a dispersion of 3 Å/mm and a resolution of 25 000 were recorded. The mean exposure time was 1.5 h, yielding final signal-to-noise ratios  $S/N = 100$ . The width of the spectra was 60 Å. Before determining the radial velocity, the spectra were centered on the HeII 4686 Å line. The radial velocity was measured using the HeI 4713.143 Å line.

Thus, we collected 502 radial-velocity measurements distributed fairly uniformly in orbital phase (Fig. 1). To reduce the influence of random errors, the radial velocities were averaged in phase intervals

with widths of 0.05 to 0.08. The mean radial-velocity curves are presented in Fig. 1b. Quantrell *et al.* [14] have shown that the errors in the observed radial velocity of the optical star due to tidal gravitational waves are random and, thus, can be suppressed by averaging over many observations.

Due to the large number of measured radial velocities (502 values) and the comparatively large half-amplitude of the radial-velocity curve for the Cyg X-1 system ( $\sim 75$  km/s), the relative errors of the normal points in the mean observed radial-velocity curve are small ( $\sim 3\%$ ). This provides hope of being able to simultaneously estimate the black-hole mass and orbital inclination based on this radial-velocity curve.

### 3. INTERPRETATION OF THE AVERAGE RADIAL-VELOCITY CURVE

The optical component in the close binary Cyg X-1 approximately fills its critical Roche lobe [15]. Due to the tidal action with the relativistic companion, the shape of the optical component is not spherical. The side facing the relativistic component is heated by X-ray radiation. These effects must be taken into consideration when interpreting the observed radial-velocity curve. We accordingly fit the curve in a Roche model, which enabled us to implement a first approximation to include these effects. A detailed description of the Roche model is presented in [16], and we do not repeat this information here. The numerical values of the parameters for the X-ray binary Cyg X-1 are summarized in Table 2.

The orbit was taken to be circular, since the orbital period ( $P_{orb} \simeq 5^d6$ ) is comparable to the periods of the X-ray binaries SMC X-1 ( $P_{orb} \simeq 3^d9$ ) and 4U 1538-52 ( $P_{orb} \simeq 3^d7$ ), whose orbits are circular, according to the results of timing measurements for X-ray pulsars [18, 19]. The coefficient of asynchronism of the rotation  $f$  was taken to be 0.95, in accordance with the results of Gies and Bolton [3], whose analysis of the profile of the HeI 4471 Å line led them to conclude that the coefficient of asynchronism was close to unity. This also supports our assumption that the orbit is circular [20, 21]. Since the radius of the optical star is more than 0.25 of the radius of the relative orbit of the system, we can assume that the orbit of the Cyg X-1 system has had time to circularize since the formation of the black hole [20, 21]. It is not possible to accurately determine the eccentricity  $e$  from the radial-velocity curve of the optical star due to the effect of the anisotropy of the stellar wind (for more details, see [13, 22]).

The masses of both components and the orbital inclination were treated as unknown parameters. We

**Table 2.** Parameters used to synthesize the radial-velocity curves of the optical component of Cyg X-1 in the Roche model

$P$ , days	5.599829	Period
$e$	0.0	Eccentricity (postulated)
$i$ , deg	30, 35, 40 45, 55, 65	Orbital inclination
$\mu$	0.95*	Roche-lobe filling by the optical component
$f$	0.95	Asynchronism of rotation of the optical component
$T_{\text{eff}}(\text{K})$	32 000**	Effective temperature of the optical component
$\beta$	0.25	Gravitational darkening
$k_x$	0.02	X-ray luminosity of the relativistic component/ bolometric luminosity of the optical component, $L_x/L_v$
$A$	0.5	Reprocessing of the X-ray radiation
$u$	0.3***	Limb darkening

\* Data taken from [15].

\*\* Data taken from [4].

\*\*\* Data taken from [17].

obtained multiple solutions of the direct problem using various parameter values. A series of masses of the compact object  $m_x$  were considered for each mass of the optical component  $m_v$  from the discrete set of values 20, 30, 40, 50, 60, and  $70M_{\odot}$  for a specified orbital inclination  $i$ . This yielded the dependences of the mass of the compact object on the mass of the optical component for  $i = 30^{\circ}$ ,  $35^{\circ}$ ,  $40^{\circ}$ ,  $45^{\circ}$ ,  $55^{\circ}$ , and  $65^{\circ}$ .

The residual between the mean observed radial-velocity curve and the theoretical curve was calculated using the formula

$$\Delta m_x = \frac{\sum_{j=1}^M (n_j - 1) \sum_{j=1}^M n_j (V_j^{\text{teor}} - \bar{V}_j^{\text{obs}})^2}{M \sum_{j=1}^M n_j (n_j - 1) \sigma_j^2}, \quad (1)$$

where  $\bar{V}_j^{\text{obs}}$  is the observed mean radial velocity in a phase interval centered at  $\bar{\phi}_j$ ,  $V_j^{\text{teor}}$  is the theoretical radial velocity at this phase,  $\sigma_j$  is the rms deviation for  $\bar{V}_j^{\text{obs}}$  in the given phase interval centered at  $\bar{\phi}_j$ ,  $M$  is the number of phase intervals, and  $n_j$  is the number of averaged observations of the radial velocity in a given phase interval.

The quantity  $\Delta(m_x)$  is distributed according to a Fisher law,  $F_{M, \sum_{j=1}^M (n_j - 1), \alpha}$  [23]. If the significance level  $\alpha$  is specified, we can find a confidence set for the unknown parameter  $m_x$  for fixed values of  $i$  and  $m_v$ .

This set is composed of values of  $m_x$  for which the following condition is satisfied [24]:

$$\Delta m_x \leq F_{M, \sum_{j=1}^M (n_j - 1), \alpha}.$$

In addition to the Roche model, we also found solutions using a point-mass model. The results were used to reveal discrepancies between the models.

Let us discuss the stellar wind from the optical component in the Cyg X-1 binary in more detail. The optical star is an O supergiant. The nonuniformity of the gravitational force at its surface and heating of the surface facing the relativistic companion disrupt the isotropy of the stellar-wind outflow. The wind velocity increases near the Lagrange point  $L_1$ . This is manifest as an excess negative radial velocity near phase 0.5, when the X-ray source is in front of the O supergiant (Fig. 1). A detailed analysis of the anisotropy of the stellar wind in an X-ray binary with OB supergiants was carried out in [13]. This anisotropy leads to systematic errors in the observed radial-velocity curve. We accordingly used the following two methods to fit the mean radial-velocity curve.

*Method 1.* Using all the averaged observed radial velocities.

*Method 2.* Excluding the observed radial velocities at phases 0.4–0.6, since they are most distorted by the anisotropy of the stellar wind.

We adopted a significance level of 5%. Both the Roche and point-mass models can be rejected at a

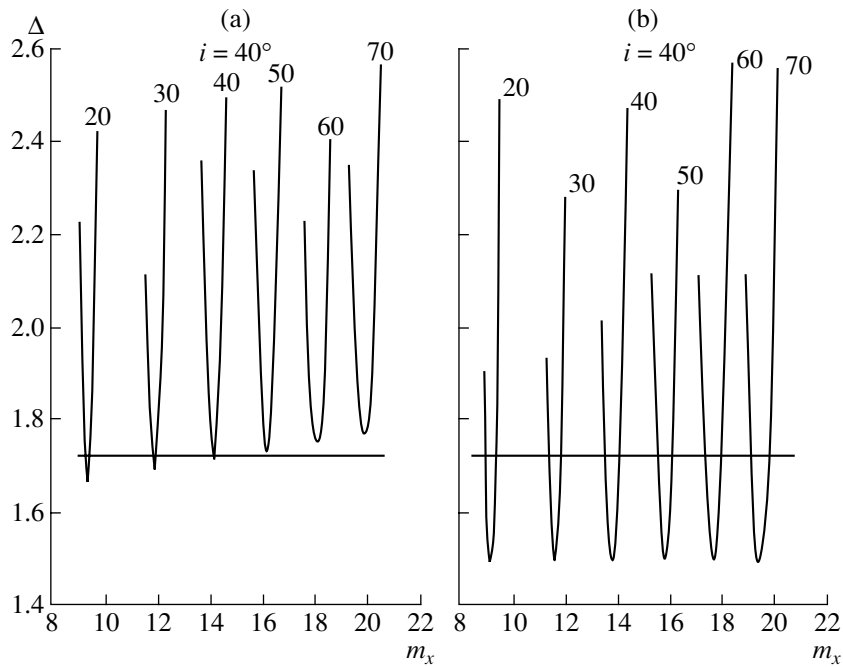


**Fig. 2.** Residuals obtained for method 2 (i.e., excluding the mean observed radial velocities at phases 0.4–0.6). Shown are the difference between the mean observed radial-velocity curve of Cyg X-1 and the synthesized curves for the (a) Roche model and (b) point-mass model for orbital inclination  $40^\circ$ . The horizontal line corresponds to the critical residual according to the Fisher criterion,  $\Delta_{13,401} = 1.72$  for a significance level of 5%. The masses of the optical component in solar masses for which the residuals were derived are presented near the curves.

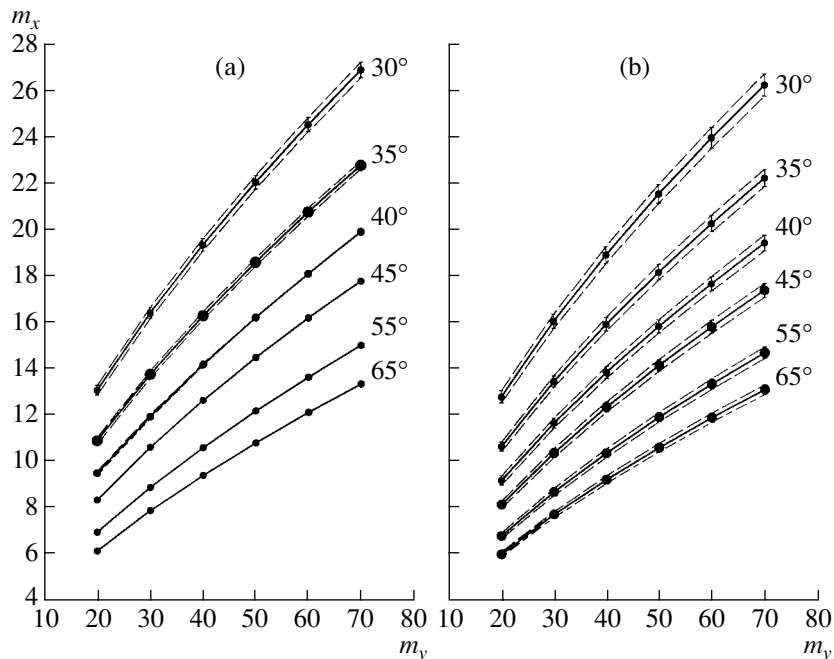


**Fig. 3.** (a) Dependence of the mass of the compact object in the Cyg X-1 binary on the mass of the optical star obtained in the Roche model using method 2 (i.e., excluding the mean observed radial velocities at phases 0.4–0.6). The orbital inclinations are shown near the curves. (b) Same dependence for the point-mass model. In this case, a model can be obtained for any orbital inclination  $i$  and the corresponding confidence interval (whose boundaries are marked by the dashed curves) estimated. Because the Roche model can be rejected for  $i \geq 45^\circ$ , confidence intervals were not determined for  $i \geq 45^\circ$  and the error band is not indicated.

**Table 3.** Dependence of mass of the relativistic component on mass of the optical component in the Roche model for  $i = 30^\circ$ – $65^\circ$ 

$m_v, M_\odot$	$m_x, M_\odot$					
	$i = 30^\circ$	$i = 35^\circ$	$i = 40^\circ$	$i = 45^\circ$	$i = 55^\circ$	$i = 65^\circ$
20	$13.03^{+0.21}_{-0.21}$	$10.86^{+0.21}_{-0.21}$	$9.37^{+0.09}_{-0.09}$	8.31	6.92	6.12
30	$16.36^{+0.24}_{-0.24}$	$13.71^{+0.21}_{-0.21}$	$11.89^{+0.09}_{-0.09}$	10.58	8.85	7.84
40	$19.29^{+0.27}_{-0.26}$	$16.24^{+0.21}_{-0.21}$	$14.13^{+0.05}_{-0.05}$	12.59	10.56	9.36
50	$21.98^{+0.29}_{-0.30}$	$18.55^{+0.21}_{-0.21}$	16.16	14.43	12.12	10.76
60	$24.47^{+0.31}_{-0.30}$	$20.70^{+0.21}_{-0.21}$	18.06	16.14	13.58	12.06
70	$26.83^{+0.33}_{-0.33}$	$22.72^{+0.21}_{-0.21}$	19.85	17.74	14.95	13.29

**Table 4.** Dependence of mass of the relativistic component on mass of the optical component in the point-mass model for  $i = 30^\circ$ – $65^\circ$ 

$m_v, M_\odot$	$m_x, M_\odot$					
	$i = 30^\circ$	$i = 35^\circ$	$i = 40^\circ$	$i = 45^\circ$	$i = 55^\circ$	$i = 65^\circ$
20	$12.82^{+0.26}_{-0.26}$	$10.68^{+0.21}_{-0.19}$	$9.23^{+0.20}_{-0.19}$	$8.19^{+0.16}_{-0.15}$	$6.84^{+0.12}_{-0.12}$	$6.06^{+0.11}_{-0.10}$
30	$16.07^{+0.32}_{-0.31}$	$13.48^{+0.25}_{-0.24}$	$11.69^{+0.22}_{-0.20}$	$10.41^{+0.20}_{-0.18}$	$8.74^{+0.16}_{-0.16}$	$7.76^{+0.14}_{-0.13}$
40	$18.94^{+0.36}_{-0.36}$	$15.95^{+0.29}_{-0.29}$	$13.87^{+0.25}_{-0.25}$	$12.38^{+0.22}_{-0.22}$	$10.41^{+0.19}_{-0.17}$	$9.27^{+0.17}_{-0.16}$
50	$21.56^{+0.40}_{-0.41}$	$18.20^{+0.33}_{-0.33}$	$15.86^{+0.29}_{-0.27}$	$14.17^{+0.25}_{-0.26}$	$11.95^{+0.21}_{-0.20}$	$10.65^{+0.19}_{-0.18}$
60	$23.98^{+0.45}_{-0.44}$	$20.29^{+0.38}_{-0.36}$	$17.71^{+0.32}_{-0.31}$	$15.84^{+0.28}_{-0.27}$	$13.38^{+0.23}_{-0.23}$	$11.93^{+0.20}_{-0.19}$
70	$26.27^{+0.48}_{-0.48}$	$22.25^{+0.40}_{-0.36}$	$19.46^{+0.34}_{-0.34}$	$17.42^{+0.30}_{-0.30}$	$14.72^{+0.25}_{-0.25}$	$13.14^{+0.22}_{-0.21}$

significance level of  $\alpha = 5\%$  for method 1. We accordingly identified method 2 as being preferable.

Analysis of the mean observed radial-velocity curves indirectly taking into account the wind anisotropy using method 2 yielded models that were acceptable at the 5% significance level. Consequently, it is important to bear in mind the anisotropy of the stellar wind when interpreting the radial velocity curves for OB stars in close binary systems [13, 22]. The behaviors of the residuals obtained using the Roche and point-mass models for an orbital inclination of  $40^\circ$  are presented in Fig. 2. The results were used to construct the dependences of the mass of the X-ray component on the mass of the optical star (Figs. 3a and 3b). When the orbital inclination is  $40^\circ$  and the optical component mass is specified to be  $50M_\odot$ , the minimum residual occurs for  $m_x = 16.16M_\odot$  and is equal to the quantile of the critical level. Therefore, the error band in Fig. 3a is truncated at an optical-star mass of  $50M_\odot$ . At orbital inclinations of  $45^\circ$  or more, no mass of the relativistic component can fit the mean observed radial-velocity curve at the 5% significance level, as will be discussed in more detail below. Therefore, the component-mass

dependences for inclinations of  $45^\circ$ ,  $55^\circ$ , and  $65^\circ$  derived by minimizing the residuals are presented in Fig. 3a without error bands. The numerical results of fitting the mean radial-velocity curve using method 2 in the Roche model are presented in Table 3, and the results for the point-mass model are presented in Table 4. The masses of the compact object for which the models were rejected at the 5% significance level are presented in Table 3 without the confidence intervals.

Tables 3 and 4 show that the masses of the compact object obtained in the Roche model are systematically slightly greater than those obtained in the point-mass model (by  $\sim 2\%$ ).

The similarity of the masses of the compact object obtained for these two models can be explained by the following two reasons. First, the temperature of the “nose” of the optical star is lower than the temperature of most of its surface due to the low gravitational acceleration near  $L_1$  (gravitational darkening). Second, the heating of the part of the optical star facing the X-ray source is low ( $k_x = 0.02$ ). Therefore, the nose, which produces the largest perturbation to the observed radial-velocity curve, contributes only a

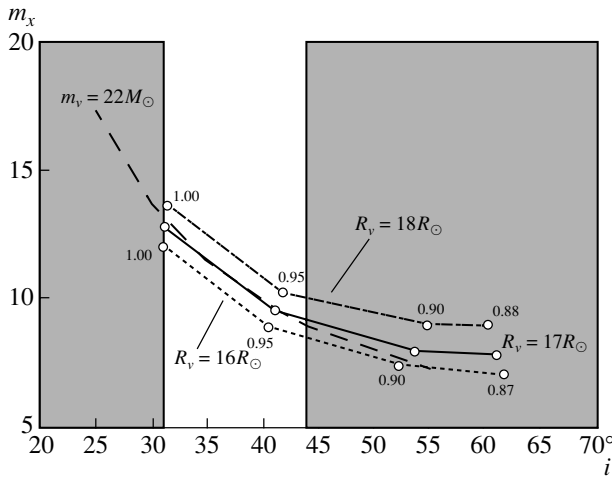


**Fig. 4.** Dependence of the mass of the compact object in Cyg X-1 on the orbital inclination. The solid, dash-dot, and dotted curves were derived from the fit to the light curve [25] with radii of the optical star equal to  $17R_{\odot}$  [4],  $18R_{\odot}$ , and  $16R_{\odot}$  [4]; the dashed curve was derived from the observed mean radial-velocity curve with the mass of the optical star equal to  $22M_{\odot}$ . The numbers near the hollow circles show the degree of filling of the Roche lobe by the optical star. Dark regions correspond to orbital inclinations that are incompatible with the light curve presented in [25] and the radial-velocity curve.

small fraction of the integrated emission of the optical component. This can explain the similarity of the results for the Roche and point-mass models. The influence of the heating coefficient on the shape of the radial-velocity curve is discussed in more detail in [1].

#### 4. MASSES OF THE COMPONENTS OF Cyg X-1

##### *Constraint on the Mass of the Black Hole from the Radial-Velocity Curve*

As follows from Fig. 3a and Table 3, the high-accuracy mean observed radial-velocity curve enables us to impose an upper limit on the orbital inclination of the Cyg X-1 binary independent of the mass of the optical star  $m_v$ :  $i < 45^{\circ}$ . This upper limit can be used to obtain a lower limit for the black-hole mass. The mass of the compact object  $m_x$  following from the mass function of the optical star  $f_v(m)$  is

$$m_x = f_v(m) \left(1 + \frac{1}{q}\right)^2 \frac{1}{\sin^3 i}. \quad (2)$$

Since  $q = m_x/m_v > 0$ , expression (2) gives

$$m_x > f_v(m) \frac{1}{\sin^3 i}, \quad (3)$$

where  $f_v(m)$  can be determined from the expression

$$f_v(m) = \frac{P(1 - e^2)^{3/2}}{2\pi G} K_v^3. \quad (4)$$

Note that the observed mass function  $f_v(m)$  corresponds to the real (nonpointlike) shape of the star and, thus, is low when compared with a point-mass model. We can take this into account when using mass function (4) by substituting the quantity  $K_v$  corresponding to the value of  $m_x$  obtained in the Roche model rather than the point-mass model. We corrected the observed value of  $f_v(m)$  for the uncertainty in the parameters of the optical star. For example, if the orbital inclination is  $i = 35^{\circ}$ ,  $f_v(m) = 0.245 \pm 0.002M_{\odot}$  in the point-mass model, while the corrected mass function is  $f_v(m) = 0.2571 \pm 0.0006M_{\odot}$ . When  $i = 40^{\circ}$ ,  $f_v(m) = 0.248 \pm 0.002M_{\odot}$  in the point-mass model, while the corrected value is  $f_v(m) = 0.2580 \pm 0.0007M_{\odot}$ . We will take the mass function of the optical component to be  $0.258M_{\odot}$ . Using this new mass function and the upper limit for the orbital inclination,  $i = 45^{\circ}$ , we can derive a lower limit on the mass of the black hole from (3). As a result, we find that the mass of the black hole in the Cyg X-1 binary is  $m_x > 0.73M_{\odot}$ . We emphasize again that this estimate was derived purely from a single high-accuracy radial-velocity curve.

##### *Estimating the Black-Hole Mass from the Radius of the Optical Component*

Fits of a high-accuracy light curve of Cyg X-1 for distances to the system of 1.5, 2.0, and 2.5 kpc, which correspond to radii of the optical component of 13.5, 18.0, and 22.5  $R_{\odot}$ , are presented in [25]. The relation between the component-mass ratio  $q$  and the orbital inclination  $i$  was determined for the corresponding degree of filling of the Roche lobe by the optical star. Analysis of the light curve presented in [25] shows that, if  $i < 31^{\circ}$ , the optical star must overflow its Roche lobe if it is to produce the observed amplitude of the optical light curve ( $\sim 0.04^m$ ). Overflowing of the Roche lobe in Cyg X-1 is unrealistic from a physical point of view, since Cyg X-1 is not associated with an object such as SS 433. If the optical star in a massive X-ray system overfills its Roche lobe, the rate of inflow of material to the accretion disk is so high that the disk becomes optically thick to X rays, and a bright optical accretion disk is observed instead of an X-ray source. Since a powerful X-ray source is observed in Cyg X-1, we can reject the hypothesis that the optical star overfills its Roche lobe. Therefore, the analysis of the light curve provides a lower limit on the orbital inclination of the Cyg X-1 binary:  $i > 31^{\circ}$ .

The analysis of spectra of the optical component in a non-LTE approximation conducted in [4] yields a radius for the optical star of  $17R_{\odot}$ . Based on this radius and the fits to the light curve from [25], we

constructed the dependence of the mass of the relativistic component in Cyg X-1 on the orbital inclination (Fig. 4). The mass of the compact object for  $q$  and  $i$  values corresponding to  $17R_\odot$  was calculated using (2). Figure 4 shows that, given the limits on the orbital inclination,  $i = 31^\circ - 44^\circ$ , the mass of the compact object obtained in [25] should be  $9.2 - 12.8M_\odot$ . We verified the dependence of the estimate of  $m_x$  on the radius of the optical star by considering two additional radii,  $16$  and  $18R_\odot$ . These  $R_v$  values were also used to construct the dependences of the black-hole mass  $m_x$  on the orbital inclination  $i$  (Fig. 4) by fitting the light curve [25]. We can see in Fig. 4 that the corresponding dependences are fairly close to each other: for the range of allowed orbital inclinations  $31^\circ < i < 44^\circ$ , the range of black-hole masses is  $8.5 - 12.0M_\odot$  and  $10.0 - 13.6M_\odot$ , respectively, for  $R_v = 16R_\odot$  and  $18R_\odot$ .

Therefore, taking the optical-star radius to be  $R_v = 17 \pm 1R_\odot$ , we find that the mass of the black hole in the Cyg X-1 binary is in the range  $m_x = 8.5 - 13.6M_\odot$ .

#### *Estimate of the Black-Hole Mass Based on Luminosity of the Optical Component*

The detailed spectroscopic analysis of [4] yielded both the radius  $R_v$  and the bolometric luminosity  $\log(L_v/L_\odot) = 5.4$  of the optical star in the Cyg X-1 system. This luminosity could then be used to obtain an estimate of the optical star's mass.

The mass–luminosity relation for the optical components of X-ray binaries differs from the relation for isolated stars [26]. An optical star in a close binary with a filled Roche lobe or an intense stellar wind loses the upper layers of its atmosphere. As a result, its surface temperature and luminosity are greater than for an isolated star of the same mass. Let us consider the mass–luminosity relation for OB supergiants in X-ray binaries (which contain X-ray pulsars for which eclipses are observed) presented in Fig. 7 of [27]. The luminosity of the optical component in Cyg X-1,  $\log(L_v/L_\odot) = 5.4$ , corresponds to the mass  $22M_\odot$ , whereas the mass–luminosity relation for noninteracting binaries gives the mass  $28M_\odot$  for the same luminosity. We will take the mass of the optical component to be  $22M_\odot$ . We used the relationship between the masses of the optical star and the compact object obtained in the Roche model (Fig. 3a) to derive the dependence of the mass of the compact object on the orbital inclination when  $m_v = 22M_\odot$  (Fig. 4). With the allowed range of orbital inclinations,  $i = 31^\circ - 44^\circ$ , the mass of the compact object should be in the range  $m_x = 9.0 - 13.2M_\odot$ .

Therefore, the black-hole masses derived from the radius of the optical component and a fit of the light

curve, on the one hand, and from the luminosity of the optical star, on the other hand, agree very well. Thus, we estimate the mass of the compact object to be  $m_x = 8.5 - 13.6M_\odot$  for the allowed range of orbital inclinations  $i = 31^\circ - 44^\circ$ .

### 5. DETERMINING THE ORBITAL INCLINATION FROM THE RADIAL-VELOCITY CURVE

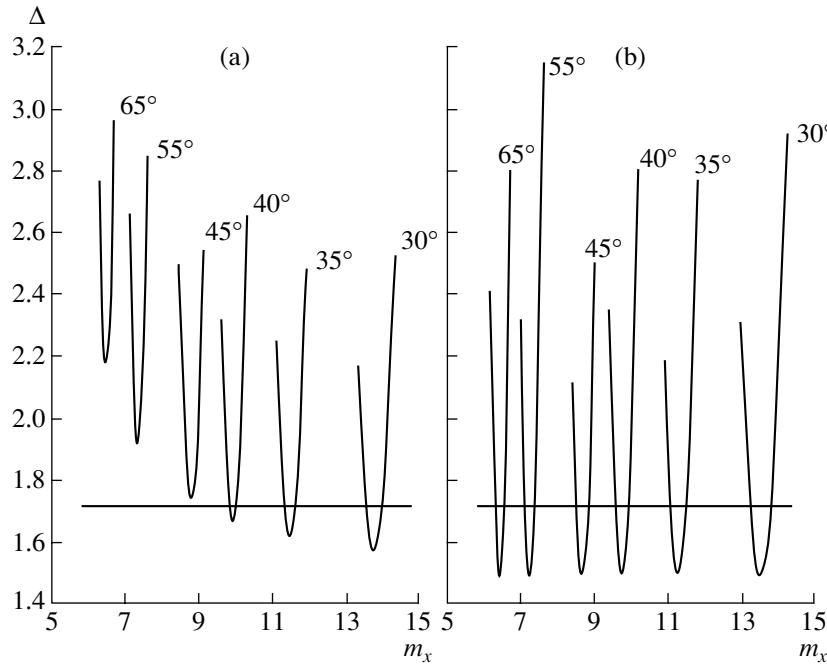
Let us consider the relations between the masses of the components derived in the Roche model for  $i = 30^\circ, 35^\circ, 40^\circ, 45^\circ, 55^\circ$ , and  $65^\circ$  (Fig. 3a). We can see that, beginning from  $i = 45^\circ$ , the theoretical radial-velocity curves cannot fit the high-accuracy mean observed radial-velocity curve at the 5% significance level for any mass of the optical star.

Figure 5a presents plots of the residuals calculated when determining the mass of the relativistic component in the Roche model for  $i = 30^\circ, 35^\circ, 40^\circ, 45^\circ, 55^\circ$ , and  $65^\circ$  and the mass of the optical component  $m_v = 22M_\odot$ . The minimum residual between the observed mean and theoretical radial-velocity curves in the Roche model increases with the orbital inclination. In other words, the model is sensitive to both the mass of the compact object and the orbital inclination. Additional calculations show that it is not possible to obtain a description of the observed mean radial-velocity curve at the 5% significance level for inclinations above  $i = 44^\circ$  and  $m_v = 22M_\odot$  for any mass of the compact object.

Figure 5b shows plots of the residuals calculated when determining the mass of the relativistic object in the point-mass model for  $i = 30^\circ, 35^\circ, 40^\circ, 45^\circ, 55^\circ$ , and  $65^\circ$  and the mass of the optical component  $m_v = 22M_\odot$ . The minimum residual is constant in this case; i.e., the model is sensitive only to  $m_x \sin^3 i$ . In other words, some mass of the compact object that satisfies the mean observed radial-velocity curve at the 95% confidence level can be determined for any orbital inclination; the minimum residual is always the same.

The possibility of determining the orbital inclination from the high-accuracy mean observed radial-velocity curve arises due to the method used to calculate the radial velocity in the Roche model. The radial velocity of a star is calculated from the shift of the integrated H $\gamma$  line profile relative to its laboratory wavelength. The position of the core of the H $\gamma$  absorption line at each phase of the orbital period is determined as the average wavelength at one-third, two-thirds, and one-half of the residual intensity of the absorption line (for more details, see [1, 16]).

If the optical star were pointlike, the profile of the absorption line would not change shape with the phase of the orbital period and the Doppler shift of the



**Fig. 5.** (a) Residual obtained by fitting the mean observed radial-velocity curve in the Roche model using method 2 (i.e., excluding the mean observed radial velocities at phases 0.4–0.6) with  $m_v = 22M_\odot$  and various orbital inclinations (the other parameters of the Roche model are listed in Table 2). The orbital inclinations are written near the curves. (b) Same for the point-mass model.

absorption-line core would correspond to the velocity of the center of mass of the star. On the other hand, since the optical component is actually a pear-shaped object with a complex temperature distribution over its surface, the absorption-line profile at each phase

differs from that formed by a point mass. The shift of the core of the  $H\gamma$  absorption line relative to the laboratory value  $4340.47 \text{ \AA}$  will no longer correspond to the velocity of the center of mass. As a result, there

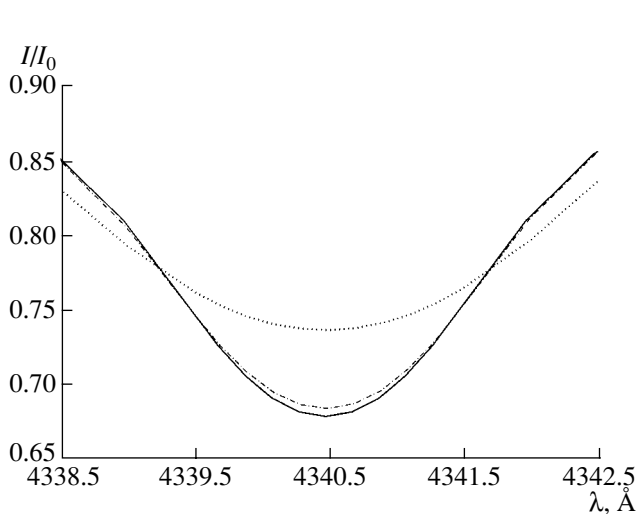


**Fig. 6.** Profile of the  $H\gamma$  absorption line in the spectrum of the optical star in Cyg X-1 for  $m_v = 22M_\odot$ ,  $m_x = 11.47M_\odot$  and  $i = 35^\circ$  at phase 0.0 (solid) and phase 0.25 (dash-dot) and for  $m_v = 22M_\odot$ ,  $m_x = 6.48M_\odot$ , and  $i = 65^\circ$  at phase 0.25.

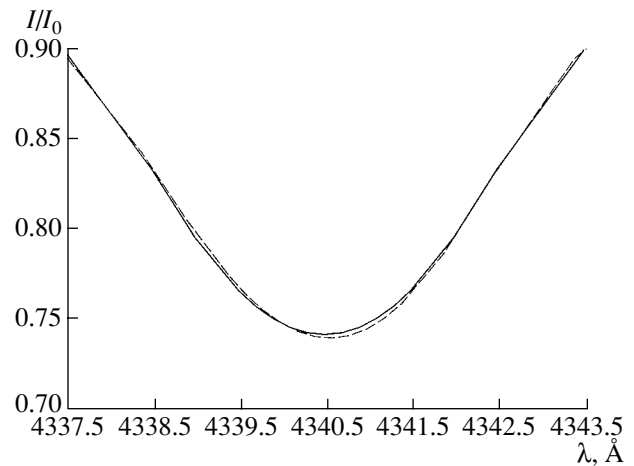


**Fig. 7.** Profile of the  $H\gamma$  absorption line in the spectrum of the optical star in Cyg X-1 for  $m_v = 22M_\odot$ ,  $m_x = 11.47M_\odot$ ,  $i = 80^\circ$ , and  $\mu = 1$  at phase 0.0 (solid) and phase 0.40 (dashed); the other parameters of the Roche model are presented in Table 2. The line profile at phase 0.40 was corrected for the Doppler shift, which was determined as the mean of residual-intensity levels of one-third, two-thirds, and one-half.

will be a discrepancy between the theoretical radial velocities in the Roche and point-mass models for a given orbital inclination.

For example, the core of the  $H\gamma$  absorption line in the point-mass model is shifted from the laboratory value by  $1.101 \text{ \AA}$  at phase 0.25, whereas the core is shifted by  $1.084 \text{ \AA}$  in the Roche model due to the asymmetry of the profile. Figure 6 presents the  $H\gamma$  profiles in the Roche model at phase 0.0 (when the optical component is in front of the compact object) and at phase 0.25 for  $m_v = 22M_\odot$  and  $i = 35^\circ$ . The  $H\gamma$  absorption profile is symmetric at phase 0.0 due to the symmetric distribution of the temperatures of the emissive regions of the optical component. At phase 0.25, the profile is asymmetric relative to the  $H\gamma$  profile at phase 0.0 (Fig. 6). To demonstrate the effect of this asymmetry more clearly, we carried out additional line-profile calculations for phases 0.0 and 0.40 for an orbital inclination of  $i = 80^\circ$ , with the optical component filling its Roche lobe ( $\mu = 1.0$ ) and the remaining model parameters equal to those for Cyg X-1 (Table 2). The synthesized profiles are presented in Fig. 7. We can see that the shape of the  $H\gamma$  profile varies with the phase of the orbital period.

Note that the theoretical profiles do not suffer from the effect of smoothing by the instrumental profile of a spectrograph, while the observed profiles used to derive the radial-velocity curve were smoothed by the corresponding instrumental profile. Since the radial velocity was measured using fairly broad hydrogen Balmer lines and HeI lines, and the resolution of the observations was high, we can disregard the effect of smoothing of the theoretical profiles by an instrumental profile.

In addition, we synthesized radial-velocity curves from the  $H\gamma$  absorption profile convolved with the instrumental profile. These calculations were carried out for two instrumental profiles with full widths at half maximum  $\text{FWHM} = 7 \text{ \AA}$  and  $\text{FWHM} = 14 \text{ \AA}$ . In a special calculation, the mass of the optical component was taken to be  $m_v = 22 M_\odot$ , keeping the other model parameters the same (Table 2). We considered a series of masses for the compact object  $m_x$  and orbital inclinations  $i = 30^\circ, 35^\circ, 40^\circ, 45^\circ, 55^\circ$ , and  $65^\circ$ . These calculations show that, as before, all models with orbital inclinations exceeding  $45^\circ$  can be rejected at the 5% significance level. The residuals between the observed radial-velocity curve obtained from the undistorted synthesized  $H\gamma$  profile and the profile convolved with the instrumental function were very similar at various values of  $i$ . Therefore, the observed radial-velocity curves of binaries with OB stars (derived from HeI lines and Balmer hydrogen lines, which are substantially broadened by the Stark effect) can be interpreted using a synthesized  $H\gamma$  absorption

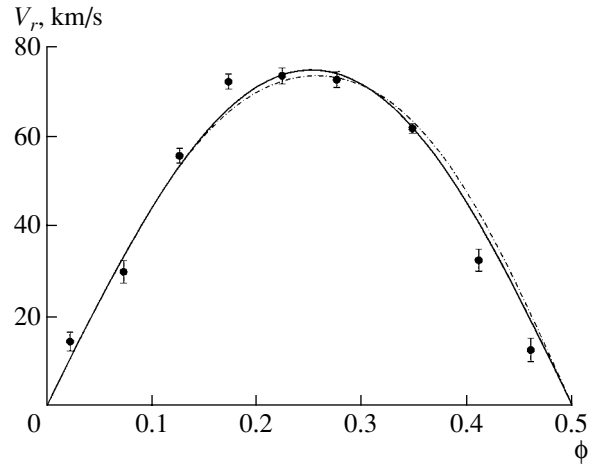


**Fig. 8.** Theoretical radial-velocity curve of the optical star in the Cyg X-1 binary calculated for the parameters corresponding to the minimum residual:  $m_v = 22M_\odot$ ,  $m_x = 11.47M_\odot$ , and  $i = 35^\circ$  (solid curve) and  $m_v = 22M_\odot$ ,  $m_x = 6.48M_\odot$ , and  $i = 65^\circ$  (dash-dot curve). The mean observed radial velocities of the optical star are shown by the points. Although the amplitudes of the best-fit radial-velocity curves are similar, the shapes of the two curves are substantially different. Precisely this fact enables us to impose constraints on the orbital inclination  $i$  using the high-accuracy radial-velocity curve.

profile, neglecting the influence of the instrumental function of the spectrograph.

In the case of a point source, if the orbital inclination is changed, the speed of the motion at a given phase will change by the ratio of the sines of the former and new orbital inclination angle (see, for example, [28]). In the Roche model, the pattern will change qualitatively when the inclination of the binary changes. Formerly hidden regions of the optical component will appear in the observer's plane of the sky, while some previously visible regions disappear. The observed line profile at a given phase will be fundamentally different (Fig. 6).

For example, when  $i = 35^\circ$  and  $m_v = 22M_\odot$ , the minimum residual in the Roche model corresponds to the mass of the compact object  $m_x = 11.47M_\odot$ . When  $i = 65^\circ$  and  $m_v = 22M_\odot$ , the minimum residual in the Roche model corresponds to  $m_x = 6.48M_\odot$ . The theoretical radial-velocity curves for these cases are presented in Fig. 8. We can see a qualitative difference between the radial-velocity curves due to the variation in the orbital inclination. When  $m_x = 6.48M_\odot$ ,  $m_v = 22M_\odot$ , and  $i = 65^\circ$ , the deviations of the radial velocities, determined by the shift of the integrated  $H\gamma$  profile relative to the observed mean velocity, are too large to be acceptable at the 95% confidence level.

Therefore, the high-accuracy radial-velocity curve and the Roche model can be used to find an upper

limit for the orbital inclination. The upper limit to the orbital inclination of the Cyg X-1 binary is  $i = 44^\circ$  for  $m_v = 22M_\odot$ . A light curve with a smaller observational error ( $\sigma \simeq 1$  km/s) would enable more precise estimation of the orbital inclination.

## 6. DEPENDENCE OF THE SHAPE OF THE RADIAL-VELOCITY CURVE ON THE ORBITAL INCLINATION

To study more carefully the effect of the orbital inclination on the shape of the radial-velocity curve in the Roche model, we calculated a series of theoretical radial-velocity curves for various orbital inclinations for both circular and elliptical orbits.

When synthesizing the radial-velocity curves for a circular orbit, the mass of the optical star was taken to be  $m_v = 22M_\odot$ , and the mass of the relativistic component, to be  $m_x = 11.47M_\odot$ . This mass of the compact object corresponds to the fit of the mean observed radial-velocity curve for orbital inclination  $35^\circ$  (Table 3, Fig. 2a). The values of other parameters of the Roche model were the same as before (Table 2). Theoretical radial-velocity curves were synthesized for orbital inclinations  $i = 30^\circ$ ,  $60^\circ$ , and  $90^\circ$ . Since the amplitude of the radial-velocity curves increases with the orbital inclination, the theoretical radial velocity was normalized to the maximum velocity in the phase interval 0.0–0.5. These normalized radial velocities for  $i = 30^\circ$ ,  $60^\circ$ , and  $90^\circ$  are presented in Fig. 9a. Due to the small magnitude of the effect, this figure presents only fragments of the relative radial-velocity curves. The shape of the curve is sensitive to the orbital inclination: the relative radial velocity of the optical star increases at phases 0.3–0.5 (and the reciprocal phase interval 0.5–0.8) with increasing  $i$ .

Theoretical radial-velocity curves for an orbit with eccentricity  $e = 0.05$  were calculated for  $m_v = 22M_\odot$  and  $m_x = 11.47M_\odot$ , which corresponds  $m_v = 22M_\odot$  in the relation between the component masses for  $i = 35^\circ$  (Fig. 2a). Radial-velocity curves for  $i = 30^\circ$ ,  $60^\circ$ , and  $90^\circ$  were synthesized for the longitudes of periastron  $\omega_v = 0^\circ$ ,  $90^\circ$ ,  $180^\circ$ , and  $270^\circ$ . The theoretical values of the radial velocity were normalized to the maximum velocity at phases 0.0–0.5. The theoretical relative radial-velocity curves for the optical star for each longitude of periastron  $\omega_v = 0^\circ$ ,  $90^\circ$ ,  $180^\circ$ , and  $270^\circ$  show variations in the shape of the radial-velocity curves, with the velocity at phases 0.3–0.5 (and the reciprocal phases 0.5–0.8) increasing with the orbital inclination. Due to the similarity of the various figures, we present here only the set of relative radial-velocity curves for  $\omega_v = 90^\circ$  (Fig. 9b). Since the effect has a small magnitude, only fragments of the curves are presented in Fig. 9b.

To complete our study of the mean observed radial-velocity curve, we estimated the eccentricity  $e$ . This search was carried out both using all the observed mean radial velocities and excluding the values at phases 0.4–0.6.

In the search for the eccentricity using all the observed mean radial velocities, we specified the mass of the optical component to be  $m_v = 22M_\odot$ . The initial value of the eccentricity was taken to be  $e = 0.05$ . The solution was found by obtaining multiple solutions of the direct problem, with the mass of the compact object being a variable parameter and the other parameters of the Roche model being the same as before (Table 2). The minimum residual, calculated using (1), was reached for the mass of the compact object  $m_x = 13.5M_\odot$  and the longitude of periastron of the optical star  $\omega_v = 270^\circ - 330^\circ$ , but this model was rejected at the 5% significance level. The mass of the compact companion for which the minimum residual was reached depended very weakly on the eccentricity and longitude of periastron of the optical component. If the eccentricity is reduced to 0.02–0.04, models with  $\omega_v = 280^\circ - 330^\circ$  and  $m_x = 13.5M_\odot$  can be accepted at the 95% confidence level. For other longitudes of periastron of the optical component, the models are still rejected. If the eccentricity continues to decrease to  $e = 0.01$ , the models are again rejected for any longitude of periastron. Therefore, we conclude that the nominal values of the eccentricity and longitude of periastron of the optical star for  $m_v = 22M_\odot$  and  $m_v = 13.5M_\odot$  are  $e = 0.03 \pm 0.01$  and  $\omega_v = 300^\circ \pm 30^\circ$ , clearly suggesting appreciable influence of anisotropy of the stellar wind on the observed radial-velocity curve [13, 22].

The search for the eccentricity excluding the mean radial velocities at phases 0.4–0.6 was carried out in the same way. The mass of the optical star was specified to be  $22M_\odot$ . The minimum residual satisfying the critical level was reached for  $m_x = 13.7M_\odot$ ,  $e = 0.01 - 0.02$ , and  $\omega_v = 300^\circ \pm 40^\circ$ . The model is rejected at the 5% significance level for all longitudes of periastron beyond  $300^\circ \pm 40^\circ$  and all significantly nonzero eccentricities.

Therefore, in the case  $e \neq 0$ , the high-accuracy radial-velocity curve of the X-ray binary likewise enables us to impose an upper constraint on the orbital inclination  $i$  in the Roche model.

## 7. CONCLUSIONS

The main results of this work are the relations between the masses of the optical and compact objects for orbital inclinations  $i = 30^\circ$ ,  $35^\circ$ ,  $40^\circ$ ,  $45^\circ$ ,  $55^\circ$ , and  $65^\circ$  (Tables 3 and 4, Fig. 3) obtained in a Roche model for the optical star.

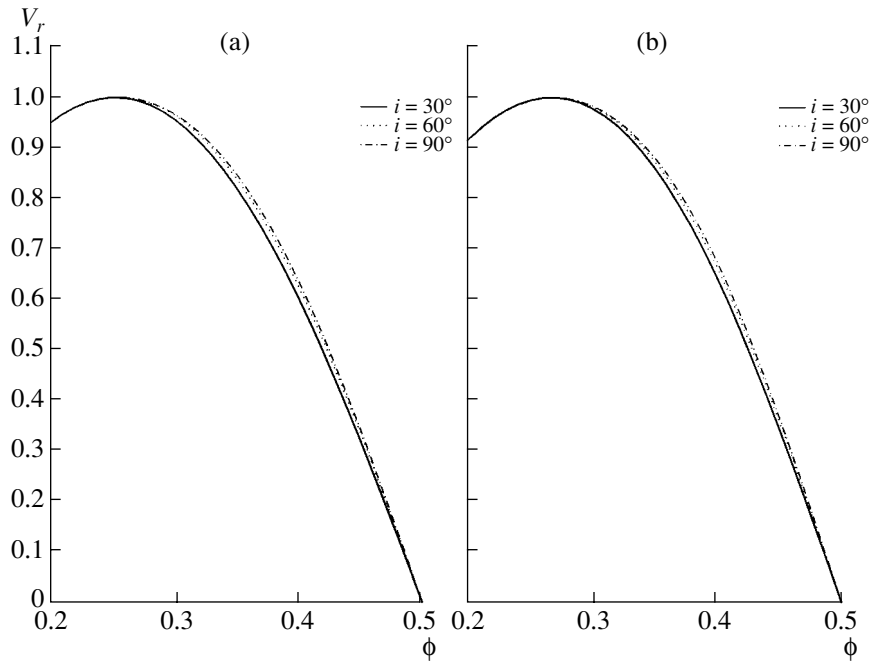


**Fig. 9.** The relative theoretical radial-velocity curves obtained in the Roche model for (a)  $m_v = 22M_\odot$ ,  $m_x = 11.47M_\odot$ , and  $e = 0.0$  for  $i = 30^\circ$ ,  $60^\circ$ , and  $90^\circ$  and (b)  $m_v = 22M_\odot$ ,  $m_x = 11.47M_\odot$ ,  $e = 0.05$ , and  $\omega_v = 90^\circ$  for  $i = 30^\circ$ ,  $60^\circ$ , and  $90^\circ$ . The remaining parameters of the Roche model are presented in Table 2. As in the case of a circular orbit, we can see the dependence of the shape of the radial-velocity curve on the orbital inclination  $i$  when  $e \neq 0$ .

Another important result is the basis this work provides for estimating the orbital inclination  $i$  from the high-accuracy radial-velocity curve of an X-ray binary in a Roche model. The relations between the masses of the compact object and optical star (Fig. 3a) show that it is possible to estimate the orbital inclination when fitting the observed radial-velocity curve in a Roche model. Due to its asymmetry, the synthesized absorption profile is fairly sensitive to variations in the inclination of the binary. For nearly any mass of the optical star, the upper limit on the orbital inclination is  $i = 45^\circ$ ; in the particular case  $m_v = 22M_\odot$ , the upper limit is  $i = 44^\circ$ .

The mass of the relativistic component was estimated using two independent methods. Using a  $B$  light curve of Cyg X-1 and the fit obtained in [25] and assuming the radius of the optical star to be  $R_v = 17 \pm 1R_\odot$  [4], we found that the mass of the compact object should be  $m_x = 8.5M_\odot - 13.6M_\odot$ . Assuming the mass of the optical component to be  $22M_\odot$  and using the mass–luminosity relation for X-ray binaries [27] yields  $m_x = 9.0M_\odot - 13.2M_\odot$ . Therefore, the black-hole masses derived from the radius of the optical component and the light curve and from the luminosity of the optical star are in good agreement. Since we do not know the exact orbital inclination, it is impossible to estimate the mass of the black hole in Cyg X-1 uniquely; we can specify only a range of possible masses. Based on the admissible interval of

orbital inclinations,  $31^\circ < i < 44^\circ$ , the mass of the compact object in the Cyg X-1 binary should be in the range  $m_x = 8.5M_\odot - 13.6M_\odot$ , which clearly exceeds the absolute upper limit on the neutron-star mass  $3M_\odot$  predicted by general relativity. When the accuracy of the observed radial-velocity curve is improved, it will be possible to more accurately estimate the orbital inclination and, consequently, the black-hole mass. In addition, accurate measurements of the distance to Cyg X-1 obtained by future space astrometric observatories (such as GAIA, SIM, etc.) will provide empirical estimates of the radius of the optical star, enabling us to resolve the question of the black-hole mass in the X-ray binary Cyg X-1.

#### ACKNOWLEDGMENTS

This work was supported by the Russian Foundation for Basic Research (project no. 02-02-17524) and by a grant from the Program of Support for Leading Scientific Schools of Russia (project NSh-388.2003.2).

#### REFERENCES

1. E. A. Antokhina and A. M. Cherepashchuyk, Pis'ma Astron. Zh. **23**, 889 (1997) [Astron. Lett. **23**, 773 (1997)].
2. T. Shahbaz, Mon. Not. R. Astron. Soc. **298**, 153 (1998).

3. D. R. Gies and C. T. Bolton, *Astrophys. J.* **304**, 371 (1986).
4. A. Herrero, R. P. Kudritzky, R. Gabler, *et al.*, *Astron. Astrophys.* **297**, 556 (1995).
5. R. E. Wilson and S. Sofia, *Astrophys. J.* **203**, 182 (1976).
6. R. J. Brucato and R. R. Zappala, *Astrophys. J.* **189**, L71 (1974).
7. H. A. Abt, P. Hintzen, and S. G. Levy, *Astrophys. J.* **213**, 815 (1977).
8. D. R. Gies and C. T. Bolton, *Astrophys. J.* **260**, 240 (1982).
9. Z. Ninkov, G. A. H. Walker, and S. Yang, *Astrophys. J.* **321**, 425 (1987).
10. J. W. Sowers, D. R. Gies, W. G. Bagnuolo, *et al.*, *Astrophys. J.* **506**, 424 (1998).
11. J. LaSala, P. A. Charles, R. A. D. Smith, *et al.*, *Mon. Not. R. Astron. Soc.* **301**, 285 (1998).
12. C. Brocksopp, A. E. Tarasov, V. M. Lyuty, and P. Roche, *Astron. Astrophys.* **343**, 861 (1999).
13. M. K. Abubekero, E. A. Antokhina, and A. M. Cherepashchuk, *Astron. Zh.* **81**, 1 (2004) [*Astron. Rep.* **48**, 89 (2004)].
14. H. Quantrell, A. J. Norton, T. D. C. Ash, *et al.*, *Astron. Astrophys.* **401**, 313 (2003).
15. A. M. Cherepashchuk, N. A. Katysheva, T. S. Khruzina, and C. Yu. Shugarov, *Highly Evolved Close Binary Stars: Catalog* (Netherland Gordon and Breach Sci., 1996), Vol. 1, Part 1, p. 82.
16. E. A. Antokhina, *Astron. Zh.* **73**, 532 (1996) [*Astron. Rep.* **40**, 483 (1996)].
17. A. A. Rubashevskii, *Astron. Zh.* **68**, 799 (1991) [*Sov. Astron.* **35**, 626 (1991)].
18. M. H. van Kerkwijk, J. van Paradijs, and E. J. Zuiderwijk, *Astron. Astrophys.* **303**, 497 (1995).
19. K. Makishima, K. Koyama, S. Hayakawa, and F. Nagase, *Astrophys. J.* **314**, 619 (1987).
20. J. P. Zahn, *Astron. Astrophys.* **57**, 383 (1977).
21. J. P. Zahn, *Astron. Astrophys.* **220**, 112 (1989).
22. M. Milgrom, *Astron. Astrophys.* **70**, 763 (1978).
23. D. Hudson, *Statistics. Lectures on Elementary Statistics and Probability* (Geneva, 1964; Mir, Moscow, 1970).
24. A. M. Cherepashchuk, *Astron. Zh.* **70**, 1157 (1993) [*Astron. Rep.* **37**, 585 (1993)].
25. N. I. Balog, A. V. Goncharskii, and A. M. Cherepashchuk, *Pis'ma Astron. Zh.* **7**, 605 (1981) [*Sov. Astron. Lett.* **7**, 336 (1981)].
26. J. Ziolkowski, *Nonstationary Evolution of Close Binaries*, Ed. by A. N. Zitkov (PWN, Warsaw, 1978), p. 29.
27. M. K. Abubekero, *Astron. Zh.* (2004, in press).
28. A. V. Goncharskii, A. M. Cherepashchuk, and A. G. Yagola, *Incorrect Problems in Astrophysics* (Nauka, Moscow, 1985), p. 54 [in Russian].

*Translated by Yu. Dumin*